Indian Journal of Pure & Applied Physics
Vol. 56, November 2018, pp. 890-895

Structural, elastic and magnetic properties of spinel Co_3O_4

P L Meena[a]*, Ravi Kumar[b] & K Sreenivas[c]

[a]Department of Physics, Deen Dayal Upadhyaya College, University of Delhi, New Delhi 110 078, India
[b]Centre for Material Science and Engineering, National Institute of Technology, Hamirpur 177 005, India
[c]Department of Physics and Astrophysics, University of Delhi, North Campus, Delhi 110 007, India

Received 30 April 2017; accepted 15 May 2018

We have investigated the structural and magnetic properties of Co_3O_4 ceramic synthesized by solid state reaction method. Powder X-ray diffraction (XRD), Raman spectroscopic and Fourier transforms infrared (FTIR) analysis reveals single phase formation at room temperature. Analysis of XRD data indicates that the Co_3O_4 crystallizes in cubic symmetry with face-centered cubic (fcc) Bravais lattice. Force constants and elastic properties have been estimated at room temperature using XRD and FTIR spectra and interpreted in terms of bond lengths. An octahedral broadening of the FTIR band (ν_o) and large force constant (k_o) has been observed and indicated the inverse proportionality relationship between the force constant and the bond length. The elastic moduli and Poisson's ratio uncorrected and corrected to zero porosity reveals the solidification of the Co_3O_4 ceramic sample. The field cooled (FC) and zero field cooled (ZFC) magnetization measurements using superconducting quantum interface device (SQUID) magnetometer exhibit a well-defined long-range antiferromagnetic order below transition (T_N = 40 K) temperature.

Keywords: Co_3O_4, X-ray diffraction, Rietveld refinement, Fourier transforms infrared, Raman spectra, Force constants, Elastic modulus, Anti-ferromagnetism

1 Introduction

Cubic spinel cobalt oxide exhibits interesting properties such as magnetic, electrical, electro-catalysis, negative temperature coefficient (NTC) thermistor, field-emission materials, lithium ion battery electrodes etc.[1-8]. Co_3O_4 has been investigated extensively as promising materials in gas-sensing, water oxidation super-capacitor, an effective catalyst in environmental purification and chemical engineering[8-12]. In addition to magnetic properties, Mn doped and pure Co_3O_4 have a very important multiferroic and magnetic semiconductor nature for information storage and multifunctional electronic device applications[13-16]. Co_3O_4 provides a unique structural characteristic with unlike valance ions at tetrahedral (8a) and octahedral (16b) site and make the more complicated structure for magnetic properties. Roth[17] suggested that normal cubic spinel structure bulk $CoCo_2O_4$ (AB_2O_4) behaves like an antiferromagnetic (AFM) with the Neel temperature $T_N \approx 40$ K. In cubic spinel $CoCo_2O_4$, Co^{2+} ions occupy tetrahedral A-site in high spin magnetic $e_g^4\ t_{2g}^3$ state, while Co^{3+} ions occupy the octahedral B-site are in a diamagnetic $t_{2g}^6\ e_g^0$ state due to a strong octahedral cubic field with large crystal-field splitting between t_{2g} and e_g levels in the 3d orbitals[18].

The elastic constants are very important to know the nature of the binding forces and thermal properties of the materials. Ultrasonic pulse transmission measurement methods are the most convenient technique to know their elastic and thermal properties[19,20]. However, no attempt has been made toward the study of elastic and thermal properties of Co_3O_4 ceramic sample, especially using infrared spectroscopy technique.

In this work, we report structural, elastic and magnetic properties of Co_3O_4 ceramic sample prepared by solid-state reaction method to identify the phase formation, solidification and to understand the magnetically ordered state at low temperature.

2 Experimental Details

Co_3O_4 spinel ceramic sample was prepared by conventional solid-state reaction method using cobalt (II, III) oxides powder as high purity (>99.97%) material. The detailed preparation method of Co_3O_4 is discussed in literature[13,21,22]. Powder X-ray diffraction pattern was recorded at room temperature using a X'PERT-PRO diffractometer (CuK_α radiation) having

*Corresponding author
(E-mail: plmeena@gmail.com, plmeena@ddu.du.ac.in)

Panalytical measurement program in the 2θ range from 15° to 80°. FTIR and Raman spectra were recorded using a Perkin Elmer RX-1 FTIR spectrometer and a Renishsaw InVia reflex micro Raman spectrometer, respectively. Magnetization measurements were performed using Quantum Design MPMS superconducting quantum interface device (SQUID) magnetometer with typical sensitivity of 10^{-7} emu in practice.

3 Results and Discussion

The crystal structure and single-phase formation of ceramic powder sample are investigated using powder X-ray diffraction (XRD) at room temperature. The XRD pattern for Co_3O_4 system shows the formation of a single phase, and all the observable reflections planes could be indexed as in Fig. 1 and are in agreement with the ICDD file PDF#413003 and earlier reported results[22,23].

The identification of the Bravais lattice can be done by the systematic presence or absence of the Bragg reflections in the observed diffraction patterns. The reflection planes (*hkl*) are unmixed (all odd or all even as shown in Fig. 1) and the sequence of $h^2+k^2+l^2$ values in the observed powder XRD pattern is 3, 8, 11, 12, 16, 24, 27, 32, 35, 40, 43 and 44, indicating the face-centered cubic (fcc) structure of the polycrystalline Co_3O_4 ceramic sample.

The lattice parameter '*a*' was calculated through the following equation[24]:

$$sin^2\theta = \left(\frac{\lambda}{2a}\right)^2 \left(h^2 + k^2 + l^2\right) \quad \ldots (1)$$

where θ is the half of the Bragg reflection angle, λ = 1.54056 Å wavelength for CuK_α radiations. The value of '*a*' is calculated by finding the slope (as shown in Fig. 2) from the linear fit of Eq. (1) using different *h*, *k*, *l* and θ values from Fig. 1. The slope of linear fit was 0.00908 which in turn gives the value of lattice parameter, *a* = 8.084 Å.

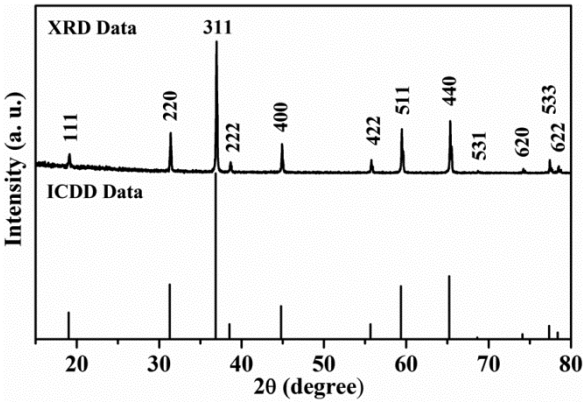

Fig. 1 – Powder X-ray diffraction pattern collected at room temperature and ICCD data for Co_3O_4.

The obtained XRD pattern of polycrystalline ceramic sample was further analyzed with Rietveld profile refinement method using FullProf suite software. The Rietveld profile fitting for Co_3O_4 sample is presented in Fig. 3 and the profile fitting quality on the experimental data was confirmed on the basis of goodness of fit (GoF = 1.25), Durbin-Watson statistic (D.W. Stat. = 1.904) and weighted-profile factor (Rp = 14.8%). The Rietveld analysis confirms the single-phase formation with spatial group $Fd\bar{3}m$ (No. 227).

An information extracted from the XRD data through Rietveld refinement method for different wavelengths ($CuK_{\alpha1}$ and $K_{\alpha2}$ =1.50433 Å) were used

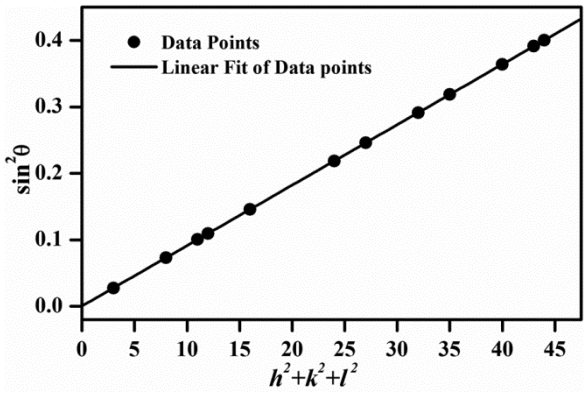

Fig. 2 – Variation of $\sin^2\theta$ versus $(h^2 + k^2 + l^2)$ for Co_3O_4 ceramic sample.

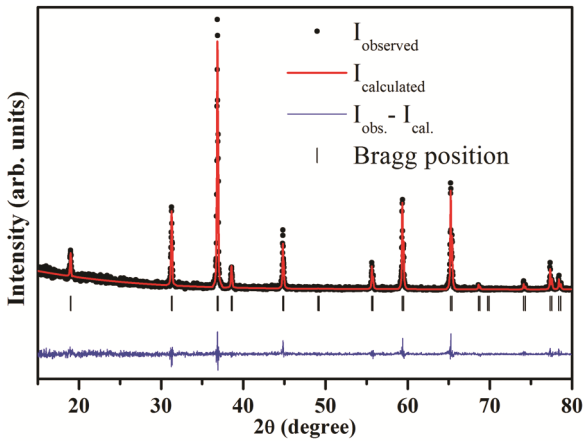

Fig. 3 – Rietveld refinement results of XRD data for Co_3O_4 ceramic sample, observed intensity patterns ($I_{observed}$, black dots), calculated intensity patterns ($I_{calculated}$, continuous red line) and difference of observed and calculated intensity patterns ($I_{obs.} - I_{cal.}$, continuous blue line). Vertical markers (black lines) indicate the position of the calculated Bragg reflection positions.

to calculate the more accurate lattice parameters '*a*' by using Cohen's method[25]:

$$A\sum\alpha^2 + B\sum\alpha\,\delta = \sum\alpha\sin^2\theta \quad \ldots (2)$$

$$A\sum\alpha\,\delta + B\sum\delta^2 = \sum\delta\sin^2\theta \quad \ldots (3)$$

where $A = \lambda/4a^2$, $\alpha = (h^2+k^2+l^2)$, $B = D/10$, and $\delta = 10\sin^2 2\theta$. The lattice parameter is calculated theoretically by using the following equation[26]:

$$a_{th} = \frac{8}{3\sqrt{3}}\left[(r_A + R_o) + \sqrt{3}(r_B + R_o)\right] \quad \ldots (4)$$

where r_A (Co^{2+} = 0.735 Å) and r_B (Co^{3+} = 0.525 Å) are the mean ionic radii of tetrahedral and octahedral sites. R_o (O^{2-} = 1.32 Å) is radius of oxygen ion.

The lattice parameter, *a*, estimated from the Eqs (1)-(3) and by Rietveld refinement method is equal to 8.084 ± 0.001 Å, and is in agreement with the theoretically calculated value and earlier reported results[22,23].

The theoretical density of the sample was calculated from the molecular weight and the volume of the unit cell[21,24] and also the bulk density of the sintered pellet was measured using Archimedes principle with distilled water. The theoretical and bulk density is found to be 6.053 g/cm^{3}and 5.980 g/cm^3 and representing porosity (P = 1.21%) in the prepared sample.

The crystallite size and lattice strain can be calculated from the Willamson-Hall equation[27] for all reflections in Fig. 1 and can be written as;

$$\beta\cos\theta = \eta\sin\theta + \frac{0.94\,\lambda}{L} \quad \ldots (5)$$

where β is the full width at half maximum (FWHM), θ is the half of the diffraction angle, η is the lattice strain, λ is the wavelength of the X-rays and L is the crystallite size. In Eq. (5), a plot of βcosθ versus sinθ yields a straight line with a slope η and intercept of 0.94λ/L. Figure 4 shows a Williamson–Hall plot using XRD data. The crystallite size was determined to be L = 95.9 ± 1.2 nm from the intercept and strain ($\eta = 6.6 \times 10^{-4}$) for the prepared Co_3O_4 ceramic sample.

Figure 5 shows the Raman spectra of Co_3O_4 ceramic sample measured at room temperature. In Co_3O_4 spinel, the observed Raman mode at ~ 689.6 cm^{-1} (A_{1g}) is attributed to the characteristics of octahedral (CoO_6 with O^7_h symmetry) sites in the spectroscopic symmetry, and the mode at ~ 194.8 cm^{-1} (F^1_{2g}) is attributed to the tetrahedral (CoO_4) sites. Raman modes for Co_3O_4 lattice observed in the present study are in agreement with the earlier reported observations[28].

Inset of Fig. 5 shows the FTIR spectra of Co_3O_4 ceramic sample. Two distinct and sharp absorption bands at 582 cm^{-1} (ν_o) and 666 cm^{-1} (ν_t) are observed in the sample. These absorption bands originate from the stretching vibrations of the metal oxygen bond. The ν_o band at octahedral site is more broaden relative to the band ν_t at tetrahedral site (Fig. 5). The difference in frequencies between ν_o and ν_t is due to different metal oxygen bond length at octahedral and tetrahedral sites. The 582 cm^{-1} (ν_o) band is characteristic of Co^{3+} vibration in the octahedral hole, and the 666 cm^{-1} (ν_t) band is attributed to Co^{2+} vibration in the tetrahedral hole of the spinel lattice and agree with the reported literature[29]. According to Waldron[30] the force constant for tetrahedral site (k_t) and octahedral site (k_o) can be calculated by the following equations:

$$k_t = 7.62 \times M_t \times \nu_t^2 \times 10^{-4} \text{ dyne/cm} \quad \ldots (6)$$

$$k_o = 10.62 \times M_o \times \nu_o^2 \times 10^{-4} \text{ dyne/cm} \quad \ldots (7)$$

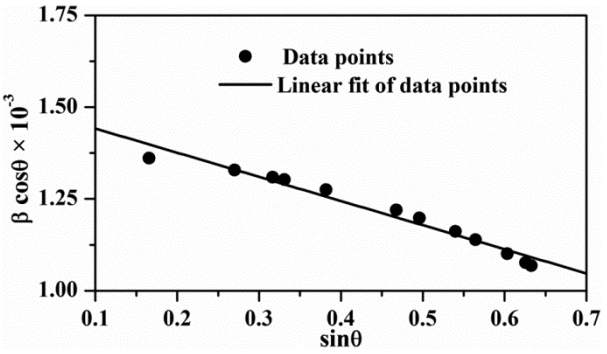

Fig. 4 – Variation of βcosθ versus sinθ for Co_3O_4 ceramic sample.

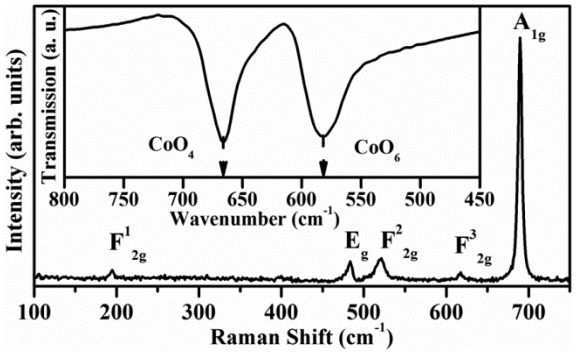

Fig. 5 – Raman spectra and inset shows FTIR spectra collected at room temperature of Co_3O_4 ceramic sample.

where M_t= 58.933 g and M_o= 117.866 g are the molecular weights of the tetrahedral and octahedral sites, respectively. The force constant for tetrahedral sites k_t = 1.992×10^4 dyne/cm and for octahedral sites and for k_o= 2.120×10^4 dyne/cm was found for $CoCo_2O_4$ system. k_o is greater than k_t, indicating that the band frequencies associated with octahedral sites are broader than the tetrahedral sites (inset of Fig. 5). This octahedral broadening of the band (v_o) and large force constant (k_o) indicate the inverse proportionality relationship between the force constant and the bond length[31]. Furthermore, the value of tetrahedral bond length (Co^{2+}- O) is larger than the octahedral bond length (Co^{3+}- O). Raman and FTIR spectra also support the formation of single phase polycrystalline nature of Co_3O_4.

The elastic moduli, Poisson's ratio and Debye temperature for porous and zero porosity were calculated (Table 1) by the formula as given in the literature[20,32,33] and more or less agree with the reported literature on Co_3O_4 determined by the resonant ultrasound spectroscopy[19]. The elastic moduli can be used to estimate the hardness and ductility of materials. In the case of spinel materials, it is usually found that the ratio of bulk to shear (B/G) modulus, called Pugh's ratio, is smaller than 1.75, indicates that the spinel oxides materials are brittle in nature[34,35]. In the present case the ratio of B/G = 1.67 was found for zero corrected porosity and similar to Co_3O_4 ceramic is consistent with the fact that spinel has a brittleness similar to that of sapphire[36]. Whereas the values of the longitudinal (V_L) and shear (V_S) elastic wave velocities determine by the average force constant $K_{average}$ = (K_t+K_o)/2 and the lattice parameter '*a*' for cubic Co_3O_4 system[30,32]. The values of V_L = 205.28 × 10^3 cm/s and V_S = 118.52 × 10^3 cm/s were found.

Figure 6 shows the temperature dependent magnetization for Co_3O_4 sample measured under the zero-field cooled (ZFC) and field cooled (FC) conditions in the presence of a 100 Oe magnetic field for temperature range 5 K ≤ T ≤ 300 K. For the ZFC case, the sample was cooled from 300 to 5 K and then a magnetic field H = 100 Oe was turned on for magnetization measurements with increasing temperature after ensuring stabilization at each temperature. Upon reaching 300 K, the data were collected with decreasing temperature (FC mode) keeping the same applied field. Co_3O_4 shows a small difference between magnetization under ZFC and FC curves at all measured temperature range indicating antiferromagnetic ordering. Ceramic sample shows the magnetization under both ZFC and FC conditions, decrease with increasing temperature after antiferromagnetic transition T_N = 40 K. This value of T_N = 40 K is in excellent agreement with the usually quoted values in the reported literature[17,37] for bulk Co_3O_4 ceramic materials.

Inset of Fig. 6 shows a variation of the inverse magnetic molar susceptibility χ_M^{-1} at 100 Oe in the temperature range from 300 K to 5 K for Co_3O_4 sample. Above the antiferromagnetic transition temperature $\chi^{-1}(T)$ increases almost linearly with the increasing temperature for ceramic sample (inset of Fig. 6), indicating a Curie-Weiss paramagnetic behavior. Indeed, the temperature dependence of susceptibility $\chi(T)$ for sample above T_N is well represented as follows[18]:

$$\chi(T) = \chi_o + \frac{C}{(T-\Theta_P)} \quad \ldots (8)$$

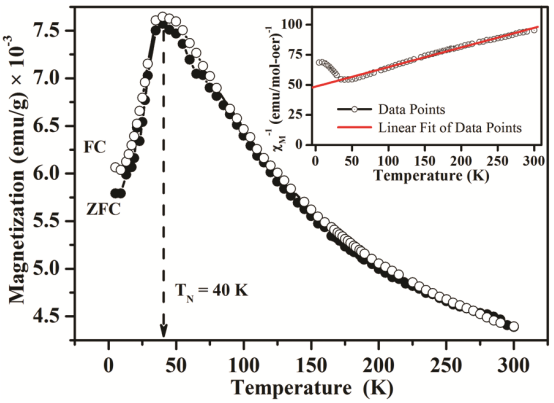

Fig. 6 – ZFC and FC magnetization as a function of temperature and inset shows inverse molar magnetic susceptibility versus temperature for Co_3O_4 sample.

Table 1 – Elastic moduli for Co_3O_4 at room temperature.

Porosity	Elastic modulus (G Pa)				Poisson's	Debye	
	Longitudinal *L*	Shear *G*	Young's *Y*	Bulk *B*	Ratio σ	Temperature θ_D	
1.21%	255.06s	85.02	212.55	141.70	0.250	143.1	This work
0%		87.08	217.82	145.65	0.251		
6.2%		74.4(1)	192.0(2)	162.6(16)	0.300(3)		Reference 19
0%		83.7(1)	219.0(2)	190.5(19)	0.308(3)		

where χ_o is the temperature independent susceptibility or paramagnetic susceptibility, C is the Curie constant, and Θ_P is the Curie–Weiss paramagnetic temperature. The temperature independent or paramagnetic susceptibility estimated from the plot $\chi_M(T) = \chi(T) - \chi_o$versus $1/T$ (not shown here) in the limit of $1/T \rightarrow 0$, using the data extracted in the high temperature region. The estimated value of $\chi_o = 7.73\pm0.23\times10^{-3}$ emu/mol-Oe was found and agrees with the reported literature[37]. The linear fit for the $\chi_M(T)$ using Eq. (8), above the transition temperature, yields the Curie - Weiss paramagnetic temperature Θ_P and Curie constant C. The estimated values of both $\Theta_P = 291.95\pm10.12$ K and $C = 6.07\pm0.16$ emuK/mol-Oe, are higher than the reported values[1,18,38] for Co_3O_4 The value of Θ_P measures the strength of the magnetic exchange interaction in the paramagnetic ($T > T_N$) regime[1,39]. An analysis of temperature dependence of the $\chi^{-1}(T)$ revealed that the Curie - Weiss temperature Θ_P is negative, indicating that strong AFM interactions exist in the single phase polycrystalline Co_3O_4 ceramic sample.

As suggested by the Roth[17], the magnetic behaviour of cubic spinel Co3O4 undergoes a magnetic transition from a high temperature paramagnetic state to a low temperature long-range ordered antiferromagnetic state at $T_N = 40$ K. Mainly, three types of magnetic interactions exist in the $Co^{2+}Co_2^{3+}O_4^{2-}$ (Co^{2+} ions are magnetic $e_g^4\ t_{2g}^3$ with high-spin S = 3/2, whereas Co^{3+} ions are in a diamagnetic $t_{2g}^6\ e_g^0$ with low-spin S = 0) state, due to a strong octahedral cubic field and consequent large crystal-field splitting between t_{2g} and e_g levels in the 3d orbitals). These exchange interactions are possible between the ions at Co^{2+} and Co^{3+}sites through the intermediate O^{2-} ions via inter-site Co^{2+} - O^{2-} - Co^{2+} and Co^{3+} - O^{2-} - Co^{3+}, and intra-site Co^{2+} - O^{2-} - Co^{3+} super-exchange interactions. The weak super exchange interaction Co^{2+} - O^{2-} - Co^{3+} - O^{2-} - Co^{2+} maintained antiferromagnetic nature[17]. The Co^{2+} - O^{2-} - Co^{2+} and Co^{3+} - O^{2-} - Co^{3+} interactions are also antiferromagnetic, but weak relative to the Co^{2+} - O^{2-} - Co^{3+} interaction. The observations seen in the present study are similar to the observation reported in literature[18], however the variation of the susceptibility χ^{-1} with temperature T indicates strong antiferromagnetic interactions exist in the spinel Co_3O_4.

4 Conclusions

In summary, single phase bulk ceramic sample of Co_3O_4 has been successfully synthesized by the solid-state reaction method. Co_3O_4 crystallizes in cubic symmetry with face-centered cubic (fcc) Bravais lattice. The value of lattice constant 8.084 Å found by experimental XRD data, Rietveld refinement, Cohen and theoretical method is same and accurate. The Rietveld analysis also confirms the single-phase formation with spatial group $Fd\bar{3}m$(No. 227). The FTIR spectra show the presence of two distinct absorption bands at 582 cm^{-1} and 666 cm^{-1}, which are attributed to the tetrahedral (Co^{2+}) and octahedral (Co^{3+}) group complexes. The force constant for tetrahedral sites 1.992×10^4 dyne/cm and for octahedral sites 2.120×10^4 dyne/cm was found for $CoCo_2O_4$ system. Large force constant (k_o) and octahedral broadening of the FTIR band (v_o) indicate the inverse relationship between the force constant and the bond length of (Co^{3+} - O). The values of elastic moduli and Poisson's ratio estimated from FTIR spectroscopy agree with the values of Co_3O_4 investigated using resonant ultrasound spectroscopy (RUS). The magnetic properties show an antiferromagnetic-type ordering and strong antiferromagnetic interactions below T_N = 40 K temperature with 6.07±0.16 emuK/mol-Oe Curie constant and 291.95±10.12 K Curie-Weiss paramagnetic temperature.

References

1 Guillemet-Fritsch S, Tenailleau C, Bordeneuve H & Rousset A, *Adv Sci Tech,* 67 (2010) 143.
2 Bordeneuve H, Guillemet-Fritsch S, Rousset A, Schuurman S & Poulain V, *J Solid State Chem,*182(2) (2009) 396.
3 Tian Z Y, Ngamou P H T, Vannier V, Kohse-Höinghaus K & Bahlawane N, *Appl Catal B Environ,* 117 (2012) 125.
4 Gao S, Jiao X, Sun Z, Zhang W, Sun Y, Wang C, Hu Q, Zu X, Yang F, Yang S, Liang L, Wu J & Xie Y, *Angew Chem Int,* 55 (2016) 698.
5 Rousset A, Tenailleau C, Dufour P, Bordeneuve H, Pasquet I, Guillemet-Fritsch S, Poulain V & Schuurman S, *Int J Appl Ceram Technol,*1 (2012) 11.
6 Varghese B, Teo C H, Zhu Y, Reddy M V, Chowdari B V R, Wee A T S, Tan V B C, Lim C T & Sow C H, *Adv Funct Mater,*17 (2007) 1932.
7 Lou X W, Deng D, Lee J Y, Feng J & Archer L A, *Adv Mater,* 20 (2008) 258.
8 Li W Y, Xu L N & Chen J, *Adv Fun Mater,*15 (2005) 851.
9 Feng Y, Yu X Y & Paik U, *Chem Commun,* 52 (2016) 6269.
10 Wang H Y, Hung S F, Chen H Y, Chan T S, Chen H M, & Liu B J*, Am Chem Soc,* 138, (2016) 36.
11 Kandalkar S G, Gunjakar J L & Lokhande C D, *Appl Surf Sci,* 254 (2008) 5540.
12 Pan L, Xu M & Zhang Z D, *J Clust Sci,* 21 (2010) 655.
13 Meena P L, Kumar R, Prajapat C L, Sreenivas K & Gupta V, *J Appl Phys,*106 (2009) 024105.
14 Takada S, Fujii M, Kohik S, Babasaki T, Deguchi H, Mitome M & Oku M, *Nano Lett,* 1 (2001) 379.
15 Meena P L, Sreenivas K & Kumar R, *Appl Sci Lett,* 1(4) (2015) 110.

16 Meena P L, Sreenivas K & Kumar R, *Indian J Pure Appl Phys,* 52 (2014) 625.
17 Roth W L, *J Phys Chem Solids*, 25 (1964) 1.
18 Ikedo Y, Sugiyama J, Nozaki H, Itahara H, Brewer J H, Ansaldo E J, Morris G D, Andreica D & Amato A, *Phys Rev B,* 75 (2007) 054424.
19 Zhang Z, Koppensteiner J, Schranz W & Carpenter M A, *Am Mineral,* 97 (2012) 399.
20 Patil V G, Shirsath S E, More S D, Shukla S J & Jadhav K M, *J Alloys Compd,* 488 (2009) 199.
21 Meena P L, Kumar R & Sreenivas K, *Int J Phys Chem Math Sci,* 3(1) (2014)7.
22 Meena P L, Kumar R & Sreenivas K, *AIP Conf Proc,* 1512 (2013) 1204.
23 Chen Y H, Zhou J F, Mullarkey D, O'Connell R, Schmitt W, Venkatesan M, Coey M & Zhang H Z, *AIP Adv,* 5 (2015) 087122.
24 Suryanarayana C & Norton M G, *X-ray diffraction: A practical approach*, (Plenum Press: New York & London), 1st Edn, (1998) 98.
25 Cohen M U, *Rev Sci Instrum*, 6 (1935) 68.
26 Patange S M, Shirsath S E, Jangam G S, Lohar K S, Jadhav S S & Jadhav K M, *J Appl Phys,* 109 (2011) 053909.
27 Williamson G K & Hall W H, *Acta Metall,* 1 (1953) 22.
28 Hadjiev V G, Iliev M N & Vergilov I V, *J Phys C: Solid State Phys,* 21 (1988) Ll99.
29 Stoilova D & Koleva V, *Chimie Inorgnique,* 53(2) (2000) 57.
30 Waldron R D, *Phys Rev,* 99 (1955) 1727.
31 Watawe S C, Sutar B D, Sarwade B D & Chougule K, *Int J Inorg Mater,* 3 (2001) 819.
32 Ravinder D & Manga T A, *Mater Lett,* 41 (1999)254.
33 Buch J J U, Lalitha G, Pathak T K, Vasoya N H, Lakhani V K, Reddy P V, Kumar R & Modi K B, *J Phys D: Appl Phys,* 41 (2008) 025406.
34 Pugh S F, *Philos Mag,* 45 (1954) 823.
35 Frantsevich I N, Voronov F F & Bokuta S A, *Elastic constants and elastic moduli of metals and insulators handbook*, Edited by Frantsevich I N (Naukova Dumka: Kiev), (1983) 60.
36 Errandonea D, *AB_2O_4 compounds at high pressures, in pressure-induced phase transitions in AB_2X_4 chalcogenide compounds*: Vol. 189- Springer Series in Materials Science, edited by F J Manjon (Springer-Verlag: Berlin), (2014) 67.
37 Dutta P, Seehra M S, Thota S & Kumar J, *J Phys: Condens Matter,* 20 (2008) 015218.
38 Rios E, Pena O, Guizouarn T & Gautier J L, *Phys Stat Sol*, 1 (2004) S108.
39 Tristan N, Hemberger J, Krimmel A, Nidda H A K V, Tsurkan V & Loidl A, *Phys Rev B,* 72 (2005) 174404.